Magn Reson Mater Phy (2011) 24:9–18
DOI 10.1007/s10334-010-0227-6

RESEARCH ARTICLE

# Accurate assessment of carotid artery stenosis in atherosclerotic mice using accelerated high-resolution 3D magnetic resonance angiography

**David Ratering · Christof Baltes · Christine Lohmann · Christian M. Matter · Markus Rudin**

Received: 11 June 2010 / Revised: 4 September 2010 / Accepted: 6 September 2010 / Published online: 23 September 2010


**Abstract**
*Object* High-resolution magnetic resonance angiography (MRA) enables non-invasive detection and longitudinal monitoring of atherosclerosis in mouse models of human disease. However, MRA is hampered by long acquisition times putting high demands on the physiological stability of the animal. Therefore, we evaluated the feasibility of accelerated MRA using the parallel imaging technique SENSE with regard to both lesion detection and quantification.
*Materials and methods* MRA acquisitions of supra-aortic vessels were performed in $ApoE^{-/-}$ mice that have been shown to develop atherosclerotic plaques. Findings obtained from accelerated data sets were compared to fully sampled reference data sets and histology.
*Results* Our results revealed only minor differences in detecting vascular lesions for data collections accelerated by factors of up to 3.3 using a four-element coil array. For vessels with a mean lumen diameter of 500 μm, morphometry of stenotic lesions revealed no substantial deviations from reference (fully sampled) data for all investigated acceleration factors. For the highest acceleration factor of 3.3, an average deviation of the degree of stenosis of 4.9 ± 3.6% was found. Common carotid stenoses assessed by in vivo MRA displayed a good correlation with histological analyses (slope of linear regression = 0.97, $R^2 = 0.98$).
*Conclusion* According to the results of this work, we have demonstrated the feasibility and accuracy of accelerated high-resolution 3D ToF MRA in mice suitable for detailed depiction of mouse supra-aortic vessels and amenable to non-invasive quantification of small atherosclerotic lesions.

**Keywords** Mouse MRA · High-resolution MRA · Supra-aortic vessels · Atherosclerosis · Parallel imaging

D. Ratering · C. Baltes · M. Rudin
Institute for Biomedical Engineering, University and ETH Zurich, Zurich, Switzerland

D. Ratering · C. Baltes · M. Rudin (✉)
AIC, ETH Zurich Hönggerberg HCI D426,
Wolfgang-Pauli-Strasse 10, 8093, Zurich, Switzerland
e-mail: rudin@biomed.ee.ethz.ch

C. Lohmann · C. M. Matter
Cardiovascular Research, Institute of Physiology and Zurich Center for Integrative Human Physiology (ZIHP),
University Zurich and Cardiology University Hospital Zurich,
Winterthurerstrasse 190, 8057 Zürich, Switzerland

M. Rudin
Institute of Pharmacology and Toxicology, University Zurich,
Winterthurerstrasse 190, 8057 Zurich, Switzerland

## Introduction

Genetically engineered mouse models of atherosclerosis have evolved as valuable tools to study the pathophysiological mechanisms of atherogenesis and to evaluate novel diagnostic and therapeutic approaches. The potential of magnetic resonance imaging (MRI) for non-invasively visualizing plaques in the aortic arch and in common carotid arteries in atherosclerotic mice has been demonstrated [1–7]. Furthermore, magnetic resonance angiography (MRA) has recently been utilized for detecting vascular lesions in several pathologic mouse models [8]. However, these MR approaches suffer from long acquisition times and/or limited spatial resolution, which is a prerequisite for accurate imaging of the mouse vasculature and morphometric assessment of vascular lesions. The small dimensions of mouse vessels require high spatial resolution with isotropic voxel dimensions typically smaller than 100 μm for three-dimensional (3D) data. This inherently translates into long acquisition times: sampling

of $N_{PE1} \times N_{PE2}$ k-space profiles, $PE_1$ and $PE_2$ being the two phase encoding directions, is time consuming and puts high demands on the physiological stability of the animal preparation. Accelerating MR data collection using parallel imaging techniques such as SENSitivity Encoding (SENSE) [9] is an efficient strategy to reduce scan time, however, at the expense of decreased signal-to-noise (SNR) ratios. This is a particular concern in small animal imaging, which is inherently compromised by low SNR values due to the small voxel dimensions involved.

In human MRA, the combination of 3D-MRA with the parallel imaging technique SENSE has been applied to reduce data acquisition time or to improve spatial resolution of angiograms for a given measurement time, while still preserving good image quality [10]. In view of the high demands regarding sensitivity in rodent MRI and the inherent losses of SNR associated with accelerated data acquisition, the application of parallel imaging techniques in small animal MRI remains a challenge. To our knowledge, the impact of parallel imaging on high-resolution small animal MR angiography has not yet been investigated.

The aim of this work was to establish and validate an accelerated high-resolution 3D time-of-flight (ToF) MRA protocol suitable for mapping the supra-aortic great arteries in the mouse. Sensitivity and accuracy of the accelerated data acquisition scheme for detecting regions of compromised vascular patency and flow disturbances was evaluated in a frequently used mouse model of atherosclerosis, the apolipoprotein E knockout $\left(ApoE^{-/-}\right)$ mouse [11,12].

The sensitivity of fully sampled 3D ToF MRA data in detecting atherosclerotic lesions in subclavian and carotid arteries of $ApoE^{-/-}$ mice was compared with that of accelerated scans. Acceleration factors of up to 3.3 were investigated in combination with a four-element (2 × 2) receiver array. For accurate comparison, contrast-to-noise ratios (CNRs) of supra-aortic vessels detected in image data and maximum intensity projections (MIPs) as well as the quantitative evaluation of lesion dimensions such as the reduced vascular lumen and the degree of stenosis (*DoS*) were calculated. Subsequently, MRA results have been correlated with histological results.

## Materials and methods

### Animal model and preparation

All animal experiments were carried out in strict adherence to the Swiss law for animal protection. MRA acquisitions were performed on five $ApoE^{-/-}$ mice (The Jackson Laboratory, Bar Harbor, ME, USA), which were fed with a high cholesterol diet (1.25% cholesterol D12108 by Research Diets, NJ, USA) for 16 weeks, starting at an age of 8 weeks. Due to the lack of a functional *ApoE* gene, these mutant mice cannot produce the lipoprotein ApoE, which is essential for both transport and metabolism of lipids. For this reason, these mice exhibit markedly elevated plasma cholesterol levels and spontaneously develop macrophage-rich early atherosclerotic lesions in their proximal aorta at an age of 3 months, which later progress to mature plaques in the aorta as well as supra-aortic and coronary arteries [11,12].

For MRI experiments, mice were anesthetized with an initial dose of 3% isoflurane (Abbott, Cham, Switzerland) in air:$O_2$ (4:1), intubated with a tube made from polyethylene (PE; ID/OD: 0.4/0.8 mm) and artificially ventilated using a small animal ventilator (Maraltec, Alfos Electronics, Biel-Benken, Switzerland) with electronically controlled valves. Applying a respiration rate of 100–120 breaths/min, an inspiration/expiration ratio of 0.20 was required to maintain blood $CO_2$ values within the physiological range (35–40 mm Hg). Animals were positioned on a cradle made of PMMA comprising a built-in warm water circuit to maintain body temperature at 36°C. Body temperature was measured using a rectal temperature probe (MLT415, ADInstruments, Spechbach, Germany). During the experiments, anesthesia was maintained using 1.4–1.5% isoflurane in air:$O_2$ (4:1).

### Experimental setup and data evaluation

All in vivo experiments were performed on a Bruker Pharmascan 47/16 (Bruker BioSpin MRI, Ettlingen, Germany) small animal MR system operating at 200 MHz. The gradient coils are capable of a maximum gradient strength of 350 mT/m at a minimum rise time of 200 µs. A transmit-only volume resonator (75.4 mm inner diameter, active length = 70 mm) operating in quadrature mode was used for proton excitation and a receive-only four-element (2 × 2) surface coil array (outer dimensions of one coil element: 12 × 16 $mm^2$, total outer dimensions: 26 × 21 $mm^2$) for signal reception. The coil elements were bent to a cylindrical surface (radius = 10 mm) with axis parallel to the main magnetic field direction.

Low-resolution gradient echo pilot scans covering the supra-aortic vasculature were acquired in horizontal, axial and sagittal orientation. Subsequently, 3D high-resolution ToF scans were carefully planned on the pilot images and acquired using the following parameters: flow-compensated 3D-gradient echo sequence, field-of-view (FOV) = 17 (read out direction; anterior–posterior direction) × 19 ($PE_1$ direction; left–right direction) × 20 ($PE_2$ direction; head–feet direction) $mm^3$, matrix dimension = 212 × 238 × 250, voxel dimension = 80 × 80 × 80 µ$m^3$, pulse angle = 80°, TE/TR = 3.7/70 ms, number of averages = 1. A TR of 70 ms was chosen in order to permit the blood to fill the whole 3D imaging slab during one TR and hence maximizing the vessel-background contrast by avoiding blood saturation effects due to multiple excitations. Since mean blood

velocities in mouse supra-aortic vessels were shown to be in the order of 24 cm/s [13], a TR of 70 ms reduces possible blood saturation effects due to multiple excitations.

Three-dimensional ToF MRA data were collected following either a full k-space sampling scheme or k-space sampling accelerated in both phase encoding directions to improve the encoding efficiency [14]. The resulting total acceleration factors ($R$) were 2.0 ($R_{\mathrm{PE1}} = 1.25$, $R_{\mathrm{PE2}} = 1.6$), 2.6 ($R_{\mathrm{PE1}} = 1.5$, $R_{\mathrm{PE2}} = 1.75$) and 3.3 ($R_{\mathrm{PE1}} = 1.75$, $R_{\mathrm{PE2}} = 1.9$), $R_{\mathrm{PE1}}$ and $R_{\mathrm{PE2}}$ being the acceleration factors in the two phase encoding directions $\mathrm{PE}_1$ and $\mathrm{PE}_2$.

Coil sensitivity maps were estimated from separate 3D gradient echo low-resolution scans: FOV $= 17 \times 19 \times 20\,\mathrm{mm}^3$, matrix dimension $= 212 \times 42 \times 42$, voxel dimension $= 80 \times 452 \times 476\,\mu\mathrm{m}^3$, pulse angle $= 15°$, TE/TR $= 2.8/50$ ms, number of averages $= 2$, total scan time $= 2.9$ min. As the volume resonator could only be operated in transmission mode, the magnitude of the reference image was calculated as the sum-of-squares (SOS) of the single coil images and the corresponding phase was calculated according to the method proposed by de Zwart et al. [15]. In addition, the noise covariance matrix of the coil elements was estimated from a separate scan and included into the reconstruction algorithm as proposed by Pruessmann et al. [9]. SENSE reconstruction was performed on a separate workstation using in-house software written in IDL (RSI, Boulder, USA).

Reconstruction errors ($E_{R,Ref}$) confined between 0 (no reconstruction error) and 1 (maximum reconstruction error) were calculated as quantitative measure of the reconstruction quality of SENSE reconstructed images and MIPs compared to fully sampled Roemer reconstructed [16] images and MIPs, respectively, according to:

$$E_{R,Ref} = \frac{\sum_{x,y} \left| |I_R(x,y)| - \left|I_{Ref}(x,y)\right| \right|}{\mathrm{MAX}\left( \sum_{x,y} |I_R(x,y)|, \sum_{x,y} \left|I_{Ref}(x,y)\right| \right)}, \tag{1}$$

where $I_R$ and $I_{Ref}$ represent images or MIPs recorded with an acceleration factor $R$ and with full k-space coverage (reference: $Ref$), respectively. In order to restrict the error calculation on the supra-aortic vasculature and exclude regions of pure noise, intensity values $<3$ times the standard deviation of the reference data ($R = 1.0$) were excluded from the calculation of $E_{R,Ref}$ for 3D image data and MIPs, respectively.

In addition, CNR values were calculated at different levels with respect to the stenotic lesions in the image data sets and MIPs according to:

$$\mathrm{CNR} = \frac{\mathrm{MEAN}\left(S_{\mathrm{Vessel}}\right) - \mathrm{MEAN}\left(S_{\mathrm{BG}}\right)}{\mathrm{SD}\left(S_{\mathrm{BG}}\right)}, \tag{2}$$

where $S_{\mathrm{Vessel}}$ and $S_{\mathrm{BG}}$ and $\mathrm{SD}\left(S_{\mathrm{BG}}\right)$ are defined as the signal on the vessel, the background signal adjacent to the investigated vessel and the standard deviation of the background signal, respectively. Being aware that the noise distribution in SENSE reconstructed images varies spatially, we evaluated CNR between the vessel of interest and the background signal right adjacent to the vessel of interest because the ability to discriminate the vasculature from background is primarily determined by the noise level of the background signal located in the neighborhood of the examined vessel. For the CNR calculations of the 3D data sets, circular noise regions-of-interests (ROIs) surrounding the vessel of interest were chosen containing approximately 160 voxels. CNR measurements were performed for both, non-accelerated and accelerated data sets.

The mean CNR deviation ($\Delta\mathrm{CNR}_R$) from the reference value (CNR for $R = 1.0$) was calculated for all investigated acceleration factors $R$ as a measure for the CNR decrease resulting from the accelerated data collection. $\Delta\mathrm{CNR}_R$ was calculated for selected vessels at different vascular positions, i.e., at the site of maximum vessel constriction (stenosis), at proximal site (site located toward the animal heart, i.e., $-560\,\mu\mathrm{m}$ from the investigated stenotic lesion) and at distal site (site located toward the animal head, i.e., $+560\,\mu\mathrm{m}$ from the investigated stenotic lesion). Based on visual inspection, only the most prominent stenosis in each animal was selected for CNR calculation. $\Delta\mathrm{CNR}_R$ was determined according to:

$$\Delta\mathrm{CNR}_R = \frac{1}{N} \sum_{i=1}^{N} \frac{\mathrm{CNR}_{R,i} - \mathrm{CNR}_{Ref,i}}{\mathrm{CNR}_{Ref,i}} \cdot 100, \tag{3}$$

where $\mathrm{CNR}_{R,i}$ is defined as the CNR value for acceleration factor $R$ ($R = 2.0, 2.6, 3.3$), $\mathrm{CNR}_{Ref,i}$ as the CNR value for acceleration factor 1.0 for each animal $i$ and $N$ as the total number of animals ($N = 5$).

The degree of stenosis ($DoS$) as a measure for the severity of the stenosis was calculated according to:

$$DoS = \frac{\text{Cross-sectional area stenosis}}{\text{Cross-sectional area proximal site}} \cdot 100, \tag{4}$$

where proximal cross-sectional areas were calculated as the mean value of the lumen areas contained between $-400\,\mu\mathrm{m}$ and $-720\,\mu\mathrm{m}$ from the site of maximum vessel constriction. Based on visual inspection, only the most prominent stenosis in each animal was selected for $DoS$ calculation.

The effect of the accelerated data collection on the $DoS$ was investigated by estimating the deviation of the $DoS$ ($\Delta DoS_R$) from the reference value obtained from the non-accelerated acquisition ($R = 1.0$). The mean deviation of the $DoS$ was calculated over all investigated animals according to:

$$\Delta DoS_R = \frac{1}{N} \sum_{i=1}^{N} \frac{\left| DoS_{R,i} - DoS_{Ref,i} \right|}{DoS_{Ref,i}} \cdot 100, \tag{5}$$

where $DoS_{R,i}$ is defined as the degree of stenosis for acceleration factor $R$ ($R = 2.0, 2.6, 3.3$) and $DoS_{Ref,i}$ as the degree of stenosis for acceleration factor 1.0 for each animal $i$. Only the most prominent stenosis of each animal was examined.

### Quantitative histopathology

All animals were killed following the MRA experiment for histological examination in order to compare the results to 3D-MRA. For tissue fixation, the left ventricle of the heart was punctured and the right atrium was cut. Vessels were rinsed with phosphate-buffered saline (PBS) and perfusion-fixed at 100 mm Hg for 8 min using 4% paraformaldehyde (Sigma-Aldrich AG, Buchs, Switzerland) in PBS. Subsequently, supra-aortic vessels were excised and embedded in optimal cutting temperature compound (Tissue-Tek, Qiagen AG, Hombrechtikon, Switzerland), frozen and stored at −80°C.

Consecutive cross sections of 5 μm thickness were cut and stained with hematoxylin and eosin (H&E). All sections were photomicrographed with a digital camera (Olympus DP50-CU, Olympus AG, Volketswil, Switzerland) mounted on an Olympus BX51 microscope. The lumen area was measured for sections 50 μm apart using Analysis 5 (SoftImaging, Olympus AG, Volketswil, Switzerland) until the plaque could not be detected in the section anymore.

## Results

### Anatomical definition of supra-aortic vessels and vascular lesions

ToF MRA yielded 3D anatomical data depicting the mouse aortic arch and branches of subclavian and carotid arteries with high anatomical definition (isotropic voxel dimension 80 μm; Fig. 1). Representative horizontal MIPs of murine supra-aortic arteries are shown in Fig. 1 for a fully sampled acquisition and accelerated acquisitions acquired with total acceleration factors of $R = 2.0, 2.6$ and 3.3. Total data acquisition time for the fully sampled data set amounted to 69 min. Upon increasing the $R$-values, noise contributions in the MIPs increase as predicted by SENSE theory [9]. This finding is confirmed by the $E_{R,Ref}$ errors depicted in Fig. 1, which account for deviations between the non-accelerated and accelerated MIPs. Nonetheless, the definition of vascular structures was only slightly compromised by the accelerated data collection when compared with the reference data set ($R = 1.0$) as illustrated by the difference images (Fig. 1). Similarly, $E_{R,Ref}$ errors were calculated between non-accelerated and accelerated image data sets for all animals: mean reconstruction errors were calculated for all investigated acceleration factors with respect to reference ($R = 1.0$) and were found to be $0.17 \pm 0.03$ for $R = 2.0$, $0.19 \pm 0.04$ for $R = 2.6$ and $0.25 \pm 0.12$ for $R = 3.3$.

Despite the increase of reconstruction errors with increasing $R$-value, acceleration did not compromise the detectability of sites with reduced vascular patency in major arteries. For example, a stenotic lesion in the right carotid artery (RCCA, white arrow in Fig. 1) could be unambiguously depicted even for an acceleration factor of 3.3 (inserts of Fig. 1). However, the inherent CNR was not high enough to warrant detectability of small vascular structures during accelerated data acquisition. Notably, this behavior was primarily observed in the images acquired with an acceleration factor of $R = 3.3$. A representative example is shown in Fig. 2a, where vessels with diameters ≤250 μm (white arrows) are not well reproduced in the accelerated acquisition ($R = 3.3$) when compared to reference ($R = 1.0$). For this reason, 30 vessels of different size were analyzed over all animals in terms of CNR for both fully sampled and accelerated image data (Fig. 2b). As can be seen from Fig. 2b, average CNR was found to decrease as a function of vessel size defined by the number of voxels contained in the vascular cross section. When comparing data acquired with $R = 3.3$ to the reference scan with $R = 1.0$, an additional CNR decrease in the order of 47–50% has been determined for vessels containing 15– 40 voxels, i.e., with an average diameter >300 μm, which amounted to 54% for smaller vessels with an average diameter ≤300 μm (8–14 voxels) (Fig. 2b). The absolute CNR values ranged from an average maximum value of $15.09 \pm 2.98$ for the biggest vessels (35–40 voxels, average diameter >500 μm) to an average minimum value of $6.60 \pm 1.70$ for the smallest vessels (8–14 voxels) when analyzing the fully sampled acquisitions (Fig. 2b). For the accelerated acquisitions of $R = 3.3$, CNR values ranged from an average maximum value of $7.88 \pm 2.01$ for the largest vessels to an average minimum value of $3.03 \pm 0.85$ for the smallest vessels detected (Fig. 2b). Correspondingly, small vessels (8–14 voxels) with an inherent low CNR ∼ 5 in the fully sampled images where frequently missed when accelerating the data collection by $R = 3.3$: only 46% of the small vessels (8–14 voxels) detected in the fully sampled acquisitions could be unambiguously identified in the accelerated acquisitions of $R = 3.3$ (Fig. 2c). The reported CNR values were calculated using a circular noise ROI surrounding the vessel of interest and containing approximately 160 voxels. In order to examine the dependence of the CNR values on the dimension of the noise ROI, several CNR measurements were repeated for different noise ROI dimensions showing that only minor effects of the noise ROI dimension on the determination of CNR values could be found.

CNR analysis for vessels visible in the fully sampled data but not in the acquisitions accelerated by $R = 3.3$ led to a CNR threshold value of $5.2 \pm 1.1$ for vessels of fully sampled

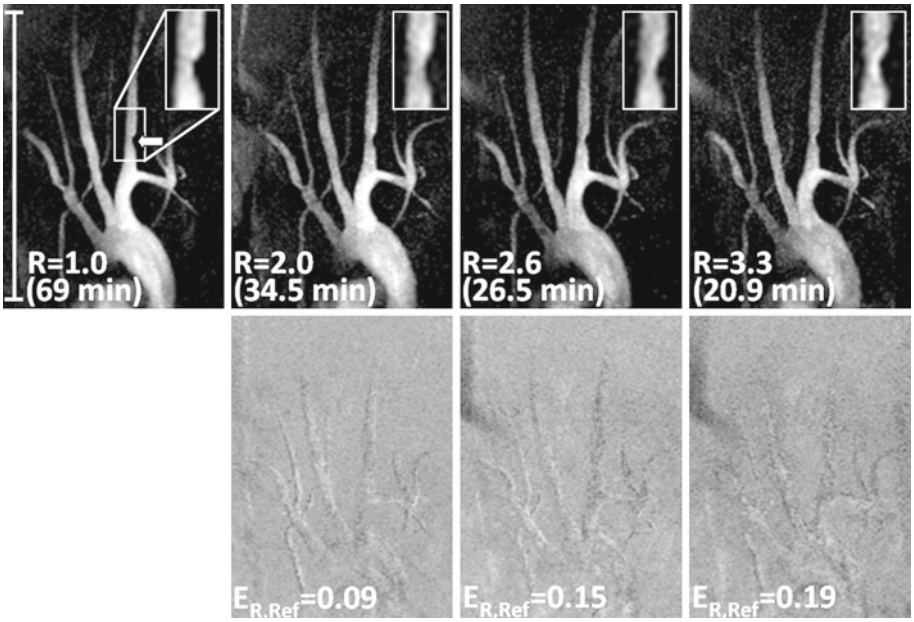


**Fig. 1** Representative horizontal maximal intensity projections (MIPs) of mouse supra-aortic vessels for different acceleration factors $R$ and corresponding difference images calculated with respect to the non-accelerated MIP ($R = 1.0$). $R$-values and corresponding acquisition times are given in the *lower left corners* of the MIPs. The *scale bar* equals 1 cm. Inserts show magnifications of the detected stenotic lesion (*white arrow*) in the right common carotid artery. Reconstruction errors were calculated between non-accelerated MIP and accelerated MIPs according to Eq. 1 and are reported in the *lower left corners* of the difference images

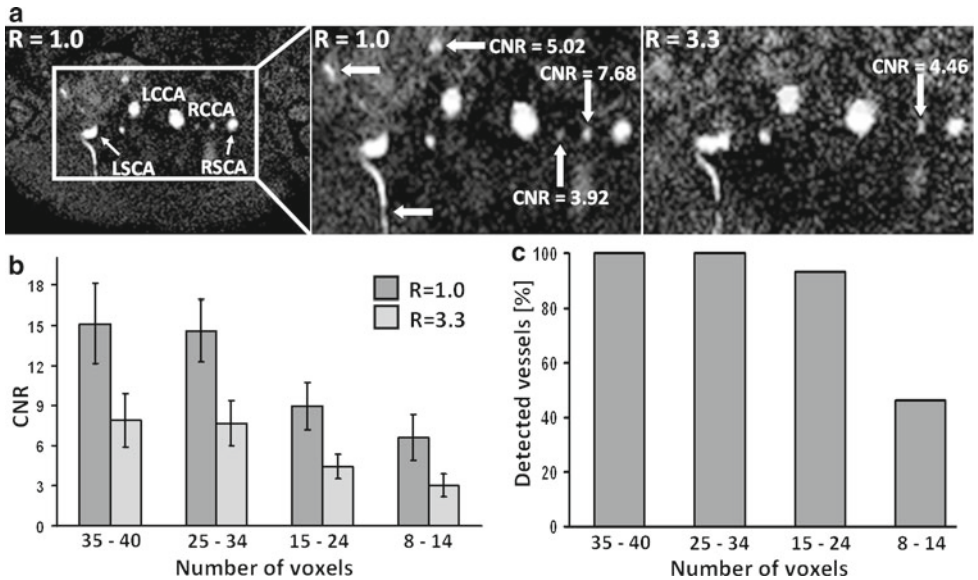


**Fig. 2** **a** Axial view of mouse supra-aortic vasculature (RCCA = Right Common Carotid Artery, LCCA = Left Common Carotid Artery, RSCA = Right Subclavian Artery, LSCA = Left Subclavian Artery) selected from a 3D image data set. Magnified views of the region indicated by the *white rectangle* are shown for an acceleration factor of $R = 1.0$ and $R = 3.3$. *White arrows* indicate vessels for which either degradation of vessel delineation is observed or for which the vessel is completely missed in the accelerated acquisition. **b** CNR decrease as function of vessel dimension (number of voxels contained in the vessel) for acceleration factors of $R = 1.0$ and $R = 3.3$. **c** Percentage of vessels detected in both, fully sampled acquisitions and acquisitions accelerated with $R = 3.3$, as function of vessel size

data. Below this CNR value, accurate representation of a vessel cannot be ensured in the accelerated image data. In addition, small vessels characterized by CNR $\geq 5$ in $R = 1.0$ data that could also be detected in accelerated scans ($R = 3.3$) displayed degraded vascular delineation. For example, the small vessel with CNR = 7.68 in the fully sampled image showed a decreased CNR value of 4.46 in the image accelerated by $R = 3.3$, leading to a visible degradation in vessel definition (Fig. 2a, middle and right panel).

Additional CNR calculations were performed for MIPs for a selected stenotic lesion in the left common carotid artery (LCCA) (Fig. 3a). Signal intensity profiles of the LCCA at the level of maximum stenosis are shown for acceleration factors $R = 1.0, 2.0, 2.6$ and 3.3 (Fig. 3b). Irrespective of the

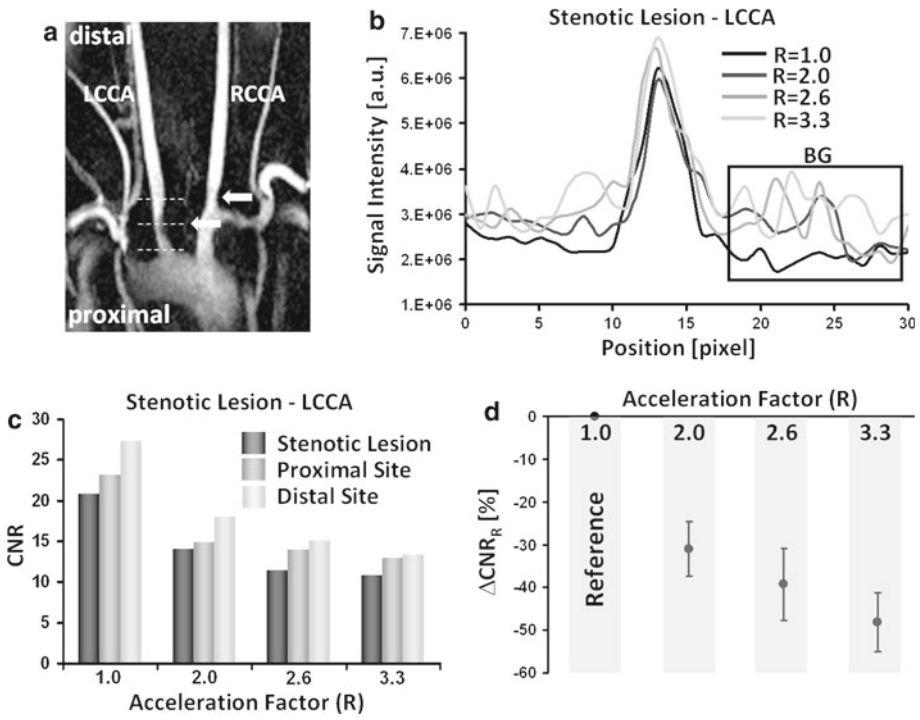


**Fig. 3** **a** Horizontal MIP of mouse supra-aortic vasculature. The *arrows* indicate the detected stenotic lesions in the left (LCCA) and right common carotid artery (RCCA) for $R = 1.0$. **b** Signal intensity profiles taken at the site of maximum vessel constriction in the LCCA. The *black rectangular box* indicates the background signal used for the CNR calculation of the stenotic lesion. **c** CNR values calculated at proximal and distal site and at the level of the stenosis (*dashed white lines* in a) for all investigated acceleration factors. **d** Mean decrease in CNR calculated with respect to reference ($R = 1.0$) for all investigated acceleration factors $R$ over all animals ($N = 5$)

acceleration factor used, the intensity profiles reproduced the reference profile obtained from fully sampled data ($R = 1.0$), the variation in maximal intensity being less than 7%. As expected, the variation of the background signal (estimated from the region indicated by the black rectangle in Fig. 3b) increased with increasing acceleration factor. This led to a decrease in CNR values at all vascular positions (Fig. 3c). Figure 3d summarizes the mean deviation of CNR from the reference value (CNR for $R = 1.0$) calculated according to Eq. 3 over all animals at different vascular positions. For $R = 3.3$, the mean CNR decrease with respect to the fully sampled acquisition amounted to 48%.

Even though CNR decreases due to inherent sensitivity losses of SENSE reconstructed data, good quality MIPs could be obtained for all acceleration factors and vessel-tissue contrast for major arterial structures (aorta, subclavian and common carotid arteries) is sufficient to allow for unambiguous delineation of vascular structures and accurate identification of stenotic lesions.

## Quantitative morphometric analysis of vascular lesions

Quantitative morphometric analysis was carried out for stenotic lesions in left and right common carotid arteries. A representative morphometric evaluation is shown in Fig. 4a, which illustrates the analysis of vascular cross-sectional areas (lumen area) at various levels relative to the stenosis in Fig. 1. Values derived from the morphometric assessment of $R = 2.0$, 2.6 and 3.3 data sets were in good agreement with readouts obtained for the non-accelerated acquisition ($R = 1.0$) as revealed from the comparison of vascular cross sections as function of distance from the center of the stenosis (Fig. 4a). The respective *DoS* values were calculated according to Eq. 4 for each acceleration factor and were found to be 57.5, 56.6, 57.1 and 55.1% for acceleration factors of $R = 1.0$, 2.0, 2.6 and 3.3, respectively.

The good agreement between non-accelerated and accelerated data is also reflected by the correlation of lumen areas determined from reference and accelerated acquisitions as illustrated by the linear regression analysis for $R = 3.3$ in Fig. 4b: a correlation coefficient of $R^2 = 0.86$ and a slope of regression line of $0.91 \pm 0.03$ could be obtained. Similar correlation coefficients could also be found for the other acceleration factors: $R^2 = 0.87$ and 0.86 were obtained for acceleration factors $R = 2.0$ and 2.6, respectively, with slopes of $0.95 \pm 0.04$ and $0.93 \pm 0.04$. When analyzing the *DoS* for stenotic lesions in all five animals, only minor deviations from the reference value ($DoS_{Ref}$ for $R = 1.0$) could be found. The corresponding results are reported in Fig. 4c: mean values of $\Delta DoS < 5\%$ were estimated for the various acceleration factors (Table 1). In addition, mean relative *DoS* values were calculated with respect to $R = 1.0$ (100%) for all animals and for all investigated acceleration factors. The results are reported in Table 1: no significant difference from the reference values were found for any acceleration factor (one population $t$ tests).

## Correlation of MRA with histopathology

In Fig. 5a, morphometric measures (lumen cross-sectional area and *DoS*) of stenotic lesions as obtained from 3D-MRA and histopathology are compared for a representative

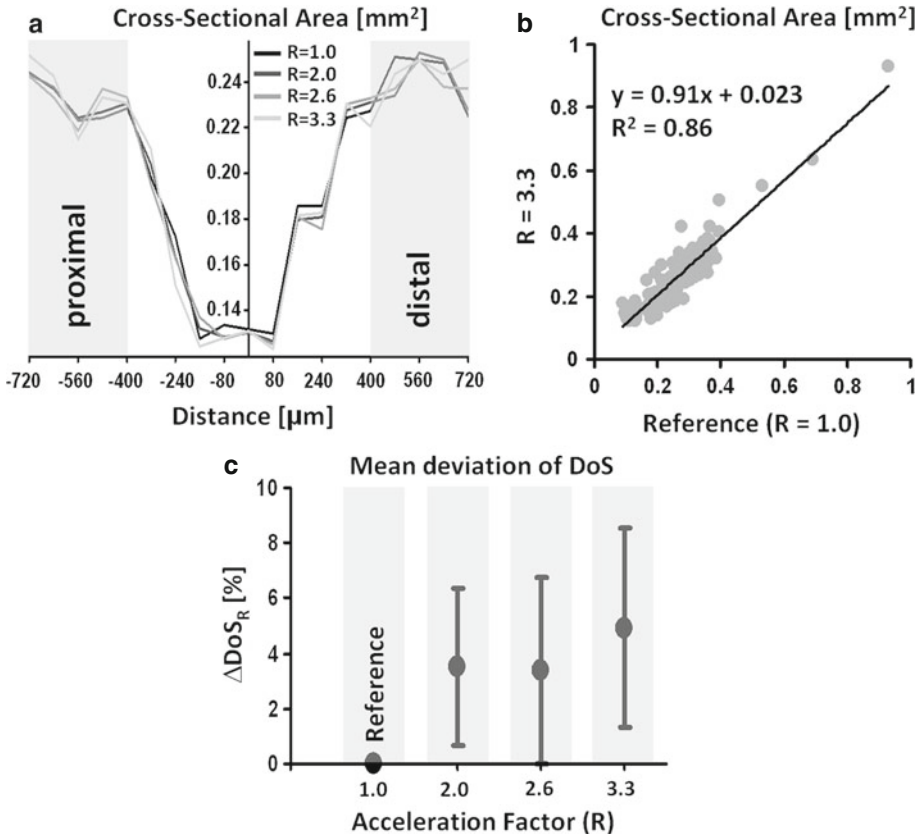


**Fig. 4** **a** Morphometric assessment of the stenotic lesion shown in Fig. 1. The graph shows vessel cross-sectional areas measured at different levels (steps of 80 µm) with regard to the stenosis for all investigated acceleration factors $R$. The corresponding degrees of stenosis ($DoS$) are 57.53, 56.63, 57.08 and 55.06% for acceleration factors of $R = 1.0$, 2.0, 2.6 and 3.3, respectively. **b** Correlation of cross-sectional lumen areas obtained from reference acquisitions ($R = 1.0$) and acquisitions accelerated by a factor of $R = 3.3$. The slope of the linear fit and the $R^2$-value indicate the degree of correlation between accelerated and non-accelerated MRA acquisition. **c** Mean deviation of degree of stenosis ($\Delta DoS_R$) from the reference value ($DoS$ obtained for $R = 1.0$) calculated for all acceleration factors over all animals ($N = 5$)

**Table 1** Quantitative assessment of degree of stenosis ($DoS$) in $ApoE^{-/-}$ mice after 16 weeks of high cholesterol diet.

| | $R = 1.0$ | $R = 2.0$ | $R = 2.6$ | $R = 3.3$ |
|---|---|---|---|---|
| Average $DoS$ (%) | 34.5 ± 15.4 | 34.1 ± 15.1 | 34.7 ± 15.5 | 33.9 ± 13.6 |
| Mean relative $DoS$ (%) | 100 | 99.0 ± 4.3 | 100.2 ± 5.1 | 100.5 ± 6.6 |
| $P$-value | – | 0.65 | 0.95 | 0.88 |
| $\Delta DoS_R$ (%) | 0 | 3.5 ± 2.9 | 3.4 ± 3.4 | 4.9 ± 3.6 |

Values represent average $DoS$, average $DoS$ relative to the reference values ($R = 1.0$) and mean deviation of $DoS$ values ($\Delta DoS_R$, Eq. 5) from the corresponding reference value ($R = 1.0$) for a given acceleration factor. Comparison reveals no significant difference between mean relative $DoS$ values for accelerated and fully sampled k-space data ($P$-values for one population $t$ tests). All values are given as mean ± SD of $N = 5$ mice

animal. Similar profiles reflecting cross-sectional areas across the stenotic lesion were found for MRA and histology, even the stepwise changes in vascular diameter on the side distal to the lesion were detected by both modalities. Similarly, the axial extent of the stenosis was almost identical both for the in-vivo MRA and the histological analysis.

The investigation of absolute values of lumen areas revealed numbers that were significantly smaller (by a factor of 2–4) for the histological evaluation when compared to the cross-sectional areas obtained from MRA. This finding was consistent for all investigated stenotic lesions and may be explained by shrinkage effects during the histological preparation. Despite differences in absolute measures of vessel cross-sectional areas, there was a good agreement between MRA and histology regarding the $DoS$ (Fig. 5a).

A correlation analysis performed in all animals is presented in Fig. 5b, c, where cross-sectional lumen areas and $DoS$ derived from MRA (for $R = 1.0$) are compared with the corresponding histomorphometric values. Due to the different slice thickness of histological and MRA data, the histological data were interpolated in order to match the corresponding MRA slice for the correlation analysis. Linear correlation analysis yielded correlation coefficients of $R^2 = 0.83$ (slope $= 2.04 \pm 0.12$, Fig. 5b) for the lumen areas and of $R^2 = 0.98$ (slope $= 0.97 \pm 0.08$, Fig. 5c) for the $DoS$. The slope in Fig. 5b indicates that vessel diameters obtained from MRA are typically 1.43 times bigger than the corresponding values obtained from histological analysis. Of note, this discrepancy in absolute values did not affect the accuracy of

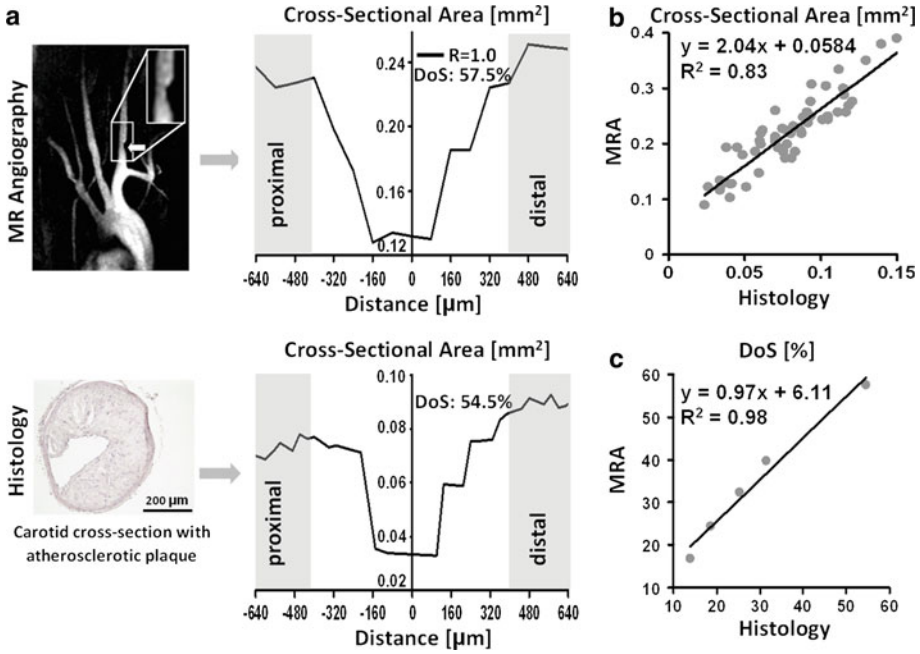


**Fig. 5** **a** Comparison of cross-sectional lumen areas and *DoS* obtained from MR angiography (*top row*, $R = 1.0$) and histology (*bottom row*) of one single mouse. Correlation of cross-sectional area **b** and of degree of stenosis **c** obtained from MRA and histology, respectively. Due to the different slice thickness of histological and MRA data, the histological data were interpolated in order to match the corresponding MRA slice for the correlation analysis. The slopes of the linear fits and the $R^2$-values indicate the degree of correlation between MRA and histology

*DoS* determinations as evident from both the slope and correlation coefficient of the respective linear curve fit (Fig. 5c).

## Discussion

$ApoE^{-/-}$ mice have been shown to develop atherosclerotic plaques that are histopathologically similar to human lesions. Hence, characterization of these lesions both with regard to composition and degree of stenosis is important for staging the disease. Non-invasive MRA in mouse models of atherosclerosis requires high (isotropic) spatial resolution, which is essential for sensitive, reliable and accurate morphometric assessment of vascular plaques in vessels with diameters of typically less than 0.5 mm. On the other hand, high spatial resolution implies long acquisition times due to the large number of sampling points, which have to be acquired. A long duration of the measurement, however, is associated with a number of disadvantages, the most trivial one being low throughput and hence lack of efficiency. More fundamental are the high demands on the physiological/metabolic stability of the animal under investigation. Stable conditions must be maintained throughout the experiment, a particular challenge when studying mouse disease models. Furthermore, animal movements should be minimized in order to optimize spatial resolution.

In this study, we have implemented and evaluated an accelerated high-resolution 3D ToF MR angiography protocol based on the SENSE technique. The accelerated acquisition scheme was optimized to maximize SNR and CNR for mapping the aortic arch as well as subclavian and common carotid arteries of mice. Significant shortening of acquisition times by factors between 2.0 and 3.3 have been achieved using this parallel 3D MRA approach, while still preserving high nominal spatial resolutions with isotropic voxel dimensions of 80 µm.

The results of this study demonstrate that high-resolution 3D ToF MRA of the aortic arch as well as subclavian and carotid arteries in mice can be successfully accelerated using SENSE even when using acceleration factors of $R = 3.3$ with a four-element coil array setup. This translates into a time reduction for measurements from 69 min ($R = 1.0$) to 21 min ($R = 3.3$). Despite significant reductions in SNR and CNR (up to 47–54% for $R = 3.3$, Figs. 2, 3), the inherent CNR is high enough so that accelerated data collection had only minor effects on image quality: high definition angiograms were obtained for murine supra-aortic vessels with diameters of 500 µm and less and vascular lesions could be reliably detected for all acceleration factors. Morphometric analyses revealed that accelerating data acquisition did not reduce the precision in assessing lumen areas and *DoS* of atherosclerotic lesions. However, accurate identification of vessels with average diameter $\leq$250 µm suffered from the decrease in overall SNR and thereby CNR associated with accelerated sampling for the highest acceleration factor of $R = 3.3$. CNR evaluations showed that an inherent CNR value >5 is required to compensate for unavoidable SNR and CNR losses of SENSE reconstructed data and hence for the correct delineation of small vessels in the

accelerated acquisitions. Small vessels detected in the fully sampled data and having CNR values slightly above 5 could also be identified using an acceleration factor of 3.3. However, this can only be achieved at the expense of degraded vessel definition. Indeed, a minimum CNR value in the order of 5 is desirable to allow for adequate signal detection by the human eye [17]. Nevertheless, as shown by the CNR evaluations of both image data and MIPs, CNR losses induced by accelerated data collection and subsequent SENSE reconstruction were less prominent for the vessels of interest being $>250\,\mu m$ in diameter. In fact, inherent CNR values were sufficiently high to compensate for SNR and CNR losses without compromising the detection and quantification of stenotic lesions, even for an acceleration factor of 3.3.

Higher acceleration factors might be achieved by the use of coil arrays with an increased number of coil elements. However, the smaller dimensions of the individual coil elements will compromise SNR, in particular for organs like the supra-aortic vessels, which are located relatively far from surface. The application of cryogenic receivers to small animal MRI has been shown to considerably increase SNR [18,19]. The extension of such cryogenic RF receiver technology to coil arrays holds promise to significantly improve SNR and hence should allow for higher acceleration factors without considerably degrading image quality.

The accuracy of the in vivo morphometric measurements of both fully sampled and accelerated MRA data is supported by the correlation of cross-sectional lumen areas and *DoS* derived from MRA with histology. An interesting observation in our study is that quantitative histological examinations revealed 2–4 times smaller lumen areas when compared to MRA. The mean vascular diameter derived from our MRA lumen areas was found to be $0.49 \pm 0.10$ mm, for diameters ranging from a minimum value of 0.34 mm to a maximum value of 1.09 mm for cross-sectional areas close to the aortic arch. These values were found in good agreement with values for the mouse common carotid artery described in the literature: vessel diameters in the range of 0.45–0.55 mm have been reported from studies using B-mode ultrasound imaging, which correspond to cross-sectional areas between 0.16 and 0.24 $mm^2$ [20]. In line with this are values reported from a study using carotid specimen with diameters of 0.40 mm with measurements taken more distally when compared to our study [21]. Similar vascular diameters have been measured in unaffected common carotid arteries of C57BL/6J and $ApoE^{-/-}$ mice with values of $0.447 \pm 0.007$ and $0.454 \pm 0.013$ mm, respectively, corresponding to lumen areas of 0.16 $mm^2$ each [22]. The significantly lower values for lumen areas determined by histology in our study are likely due to vessel shrinkage during the tissue fixation process, since the preservation of tissue vessels with formalin leads to tissue shrinkage caused by dehydration. Shrinkage effects are expected to be most prominent around vessels where the formalin concentration during perfusion fixation is highest. Indeed, similar observations have already been reported previously [23]. On the other hand, residual motion artifacts and vessel motion due to the pulsatile blood flow might lead to a slight overestimation by the in vivo method as data acquisition was not synchronized with the heart beat. Nevertheless, as shown by Jacoby et al. [8], neglecting the triggering to cardiac and respiratory motion did not compromise the quantitative assessment of vessel morphology of mouse carotid arteries. By acquiring non-gated vascular images, drawbacks associated with cardiac or respiratory triggering, such as additional increase of acquisition time and degradation of image quality in terms of SNR and CNR, could be avoided [8]. The good correlation between MRA and histology-derived values indicated that vessel shrinkage occurred to the same extent in all animals. Indeed, since the vessel shrinkage was nearly equal along the entire vessel, the calculation of the *DoS* was not affected. This is reflected by the excellent correlation of relative measurements such as the *DoS*, a parameter indicating the severity and status of atherosclerosis.

## Conclusion

In conclusion, we have demonstrated the feasibility of accelerated 3D ToF angiography in mice using the parallel imaging technique SENSE in combination with a four-element surface coil array for signal detection. The accuracy of accelerated acquisition allows the identification of supra-aortic vessels, i.e., the subclavian and common carotid arteries as well as quantification of atherosclerotic lesions. Accelerating data collection using SENSE led to considerably reduced acquisition times, while preserving high spatial resolution (isotropic voxels of $80\,\mu m$) at sufficiently high SNR and CNR for delineation of these vessels of a mean diameter of $500\,\mu m$. Quantitative morphometric analysis of stenotic lesions was not compromised by accelerating data acquisition as confirmed by comparisons with non-accelerated reference data and histology.

**Acknowledgments** We would like to acknowledge financial support by the National Competence Center for Research (NCCR), Neural Plasticity and Repair, the Swiss National Science Foundation and the University Research Priority Program “Integrative Human Physiology” at the University of Zurich.

## References

1. Fayad ZA, Fallon JT, Shinnar M et al (1998) Noninvasive in vivo high-resolution magnetic resonance imaging of atherosclerotic lesions in genetically engineered mice. Circulation 98:1541–1547

2. Manka DR, Gilson W, Sarembock I et al (2000) Noninvasive in vivo magnetic resonance imaging of injury-induced neointima formation in the carotid artery of the apolipoprotein-E null mouse. J Magn Reson Imaging 12:790–794
3. Itskovich VV, Choudhury RP, Aguinaldo JG et al (2003) Characterization of aortic root atherosclerosis in ApoE knockout mice: high-resolution in vivo and ex vivo MRM with histological correlation. Magn Reson Med 49:381–385
4. Wiesmann F, Szimtenings M, Frydrychowicz A et al (2003) High-resolution MRI with cardiac and respiratory gating allows for accurate in vivo atherosclerotic plaque visualization in the murine aortic arch. Magn Reson Med 50:69–74
5. Trogan E, Fayad ZA, Itskovich VV et al (2004) Serial studies of mouse atherosclerosis by in vivo magnetic resonance imaging detect lesion regression after correction of dyslipidemia. Arterioscler Thromb Vasc Biol 24:1714–1719
6. Alsaid H, Sabbah M, Bendahmane Z et al (2007) High-resolution contrast-enhanced MRI of atherosclerosis with digital cardiac and respiratory gating in mice. Magn Reson Med 58:1157–1163
7. Weinreb DB, Aguinaldo JG, Feig JE et al (2007) Non-invasive MRI of mouse models of atherosclerosis. NMR Biomed 20:256–264
8. Jacoby C, Boring YC, Beck A et al (2008) Dynamic changes in murine vessel geometry assessed by high-resolution magnetic resonance angiography: a 9.4 T study. J Magn Reson Imaging 28:637–645
9. Pruessmann KP, Weiger M, Scheidegger MB et al (1999) SENSE: sensitivity encoding for fast MRI. Magn Reson Med 42:952–962
10. Weiger M, Pruessmann KP, Kassner A et al (2000) Contrast-enhanced 3D MRA using SENSE. J Magn Reson Imaging 12:671–677
11. Plump AS, Smith JD, Hayek T et al (1992) Severe hypercholesterolemia and atherosclerosis in apolipoprotein E-deficient mice created by homologous recombination in ES cells. Cell 71:343–353
12. Zhang SH, Reddick RL, Piedrahita JA et al (1992) Spontaneous hypercholesterolemia and arterial lesions in mice lacking apolipoprotein E. Science 258:468–471
13. Miraux S, Franconi JM, Thiaudiere E (2006) Blood velocity assessment using 3D bright-blood time-resolved magnetic resonance angiography. Magn Reson Med 56:469–473
14. Weiger M, Pruessmann KP, Boesiger P (2002) 2D SENSE for faster 3D MRI. Magn Reson Mater Phy 14:10–19
15. de Zwart JA, van Gelderen P, Kellman P et al (2002) Application of sensitivity-encoded echo-planar imaging for blood oxygen level-dependent functional brain imaging. Magn Reson Med 48:1011–1020
16. Roemer PB, Edelstein WA, Hayes CE et al (1990) The NMR phased array. Magn Reson Med 16:192–225
17. Rose A (1948) The sensitivity performance of the human eye on an absolute scale. J Opt Soc Am 38:196–208
18. Ratering D, Baltes C, Nordmeyer-Massner J et al (2008) Performance of a 200-MHz cryogenic RF probe designed for MRI and MRS of the murine brain. Magn Reson Med 59:1440–1447
19. Baltes C, Radzwill N, Bosshard S et al (2009) Micro MRI of the mouse brain using a novel 400 MHz cryogenic quadrature RF probe. NMR Biomed 22:834–842
20. Ota R, Kurihara C, Tsou TL et al (2009) Roles of matrix metalloproteinases in flow-induced outward vascular remodeling. J Cereb Blood Flow Metab 29:1547–1558
21. Sutton MA, Ke X, Lessner SM et al (2008) Strain field measurements on mouse carotid arteries using microscopic three-dimensional digital image correlation. J Biomed Mater Res A 84:178–190
22. d'Uscio LV, Smith LA, Katusic ZS (2001) Hypercholesterolemia impairs endothelium-dependent relaxations in common carotid arteries of apolipoprotein e-deficient mice. Stroke 32:2658–2664
23. Cook NS, Zerwes HG, Pally C et al (1994) Decreased lumen size after balloon injury despite inhibition of neointimal thickening and antivasospastic treatment. Cardiovasc Res 28:215–220